University of Delaware
Newark, De 19716-3820
Ph: 302/831-6200
Fax: 302/831-6226
www.udel.edu/iec

INSTITUTE OF ENERGY CONVERSION

UNITED STATES DEPARTMENT OF ENERGY
UNIVERSITY CENTER OF EXCELLENCE
FOR PHOTOVOLTAIC RESEARCH AND EDUCATION

July 21, 2006

Ken Zweibel
National Renewable Energy Laboratory
1617 Cole Boulevard
Golden, CO 80401

Re: NREL Subcontract #ADJ-1-30630-12

Dear Ken,

This report covers research conducted at the Institute of Energy Conversion (IEC) for the period February 16, 2006 to March 15, 2006, under the subject subcontract. The report highlights progress and results obtained under Task 2 ($CuInSe_2$-based Solar Cells).

TASK 2: $CuInSe_2$-BASED SOLAR CELLS

In-Line Evaporation:Effect of heater asymmetry on film thickness uniformity

The scale-up of the $Cu(InGa)Se_2$ thin film deposition process to large area substrates and long run times is not straight forward due to the issues associated with the thermal characteristics of the source boats and the effect of melt level reduction with time. Any asymmetry in the melt temperature profile will reduce film thickness uniformity since effusion rate is directly related to the melt surface temperature. In a commercial scale process, melt depletion with time will be significant (assumed negligible for short deposition times) that may lead to unknown changes in source thermal profile and hence, melt surface temperature. During this reporting period, investigations were conducted to find out whether an asymmetric temperature profile exists in the melt and if so, what source design modification can be used to obtain a symmetric melt temperature profile.

As before, in order not to disturb the operation of IEC's in-line evaporation system, an independent vacuum bell jar system with an identical linear source was assembled to evaluate the source thermal characteristics. Fig. 1 shows schematically the evaporation source used in the present investigation as well as in the in-line system. Note that for such a source, the two nozzle effusion rates depend only on the melt temperature below the respective nozzle since the vapor flow inside the source is in transition flow regime ($0.1<K_n<10$, K_n: Knudsen number) and hence, the vapor flow conductance perpendicular (z direction) to the melt surface is much lower than the parallel (x direction).

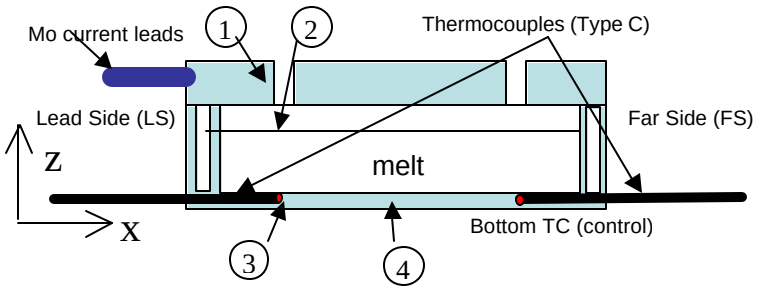

Figure 1: Thermocouple placement inside source boat.

As the first task, Femlab thermal simulation was performed to determine the thermocouple location that gives the best estimate of the melt surface temperature below the nozzle. The simulation consisted in finding the temperature response of the source in thermal equilibrium to a pulse power input. Fig. 2 shows the simulation result for an almost full source and an almost empty source. Observe that the source bottom temperature below the nozzle (dashed curve) most closely tracks the melt surface temperature below the nozzle (solid curve). For a full source, source bottom temperature is 5^oC lower than the melt surface temperature. This difference decreases to 2^oC for an empty source. Consequently, the source bottom temperature below the nozzle is used as an indication of the melt surface temperature below the nozzle.

Thermocouples located as shown in Fig. 1 were used to experimentally obtain indirect temperature measurements of the melt-surface below the two nozzles, which were then related to the respective nozzle effusion rates. The film thickness profile, which, in turn, is related to the nozzle effusion rates, is also used to determine whether the melt temperatures below each nozzle are equal. The thickness profile was obtained by depositing copper on a 10" x 1" glass substrate located directly above the source boat.

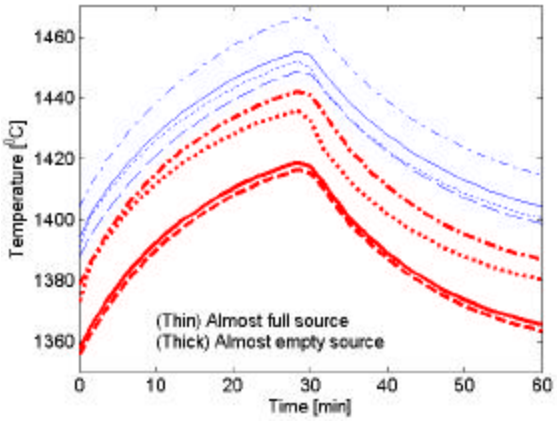

Figure 2: Temperature response of the source for a pulse power input (voltage increased by 0.5V @ t=0 and decreased by 0.5V @ t=30) using FEMLAB thermal modeling: (dotted) location 1, (solid) Melt surface temperature below nozzle (location 2), (dashed) location 3, (dash-dotted) location 4. The locations are shown in Fig. 1.

Two experimental runs were conducted with the source bottom temperature below the far side nozzle being controlled at 1400^{o}C. The lead side of the source boat was measured to be ~1370^{o}C (for Run 1) and 1375^{o}C (for Run 2), which is cooler than the far side by ~25 to 30^{o}C. Fig. 3 shows the melt surface temperature profile along the source obtained from the Femlab thermal modeling. As expected, the melt surface temperatures below the nozzles were very close to the measured temperature at the source bottom below the nozzles.

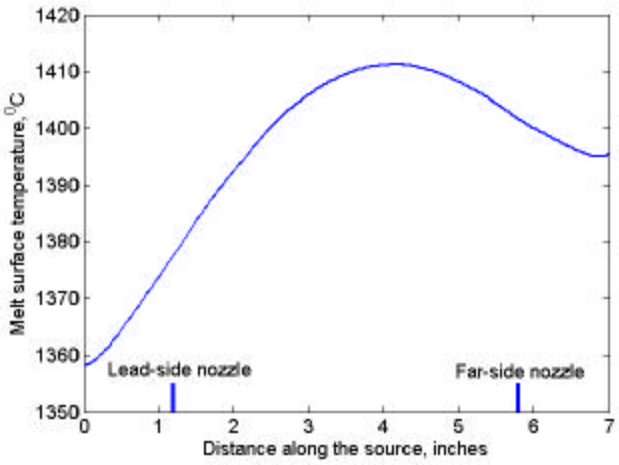

Figure 3: Melt-surface temperature profile along the source.

The nozzle-to-substrate distance was kept small (~5 inches) to increase the sensitivity of the film thickness profile on the nozzle flow rates and thus, in turn, on the melt surface temperature below the nozzles. The copper film thickness profile measured using Dektak profilometer for the two runs is shown in Fig. 4. The measurement error is ±0.1μm. Observe that the peak in the

thickness profile at the lead-side of the substrate is much lower than the far side. This can only be if a temperature difference exists on the melt surface under the lead side and far side nozzles respectively. Thus, both the temperature measurements and film thickness profile measurements show that asymmetric temperature profile exists in the melt for the present source design.

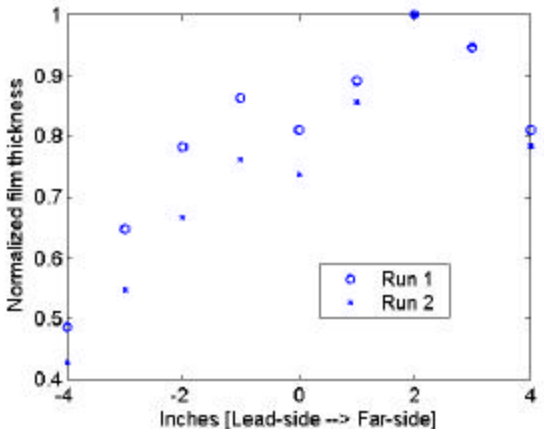

Figure 4: Experimental normalized film thickness profile across the substrate.

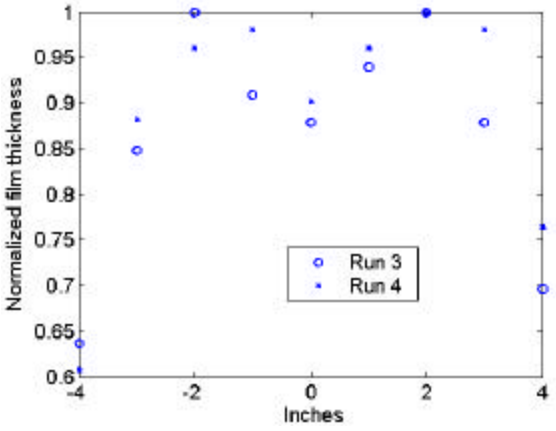

Figure 5: Normalized film thickness profile for the modified source with symmetric heater assembly.

Since the only component that is asymmetric in the source boat assembly is the heater, we presume that the heater is the main cause of the asymmetric thermal gradient in the melt. The simplest design modification to obtain a symmetric melt temperature profile is to use a symmetric heater with a power lead on each end. To verify this assertion, two experiments were performed to measure the film thickness profile for a source with symmetric heater assembly.

The experimental results are shown in Fig. 5. Observe that the film thickness profile is perfectly symmetric, signifying equal nozzle effusion rates, and hence, equal melt temperature below each nozzle. Fig. 6 shows the melt surface temperature profile along the source obtained from the Femlab thermal modeling.

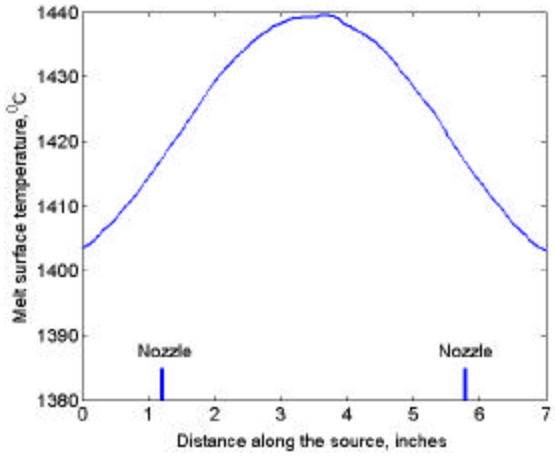

Figure 6: Melt-surface temperature profile along the source with symmetric heater.

$Cu(InGa)(SeS)_2$ Formation by H_2Se/H_2S Reaction

Efforts to characterize the reaction chemistry of $Cu(InGa)(SeS)_2$ formation by the reaction of Cu-Ga-In precursors layers in H_2Se and H_2S continue. In previous reports, we showed that a two-step reaction [1,2] could be used to control through film composition and produce devices with V_{OC} up to 0.64 V. In this work, we report the results of the 2-step reaction process with selenization at 450ºC, followed by sulfization at 550ºC, using different times for the reaction steps to further understand the process.

Experimentally, this work used $Cu_{0.8}Ga_{0.2}$/In precursor films with a composition of Cu/(In+Ga) = 0.9 and Ga/(In+Ga) = 0.2 prepared by sequential sputtering onto Mo-coated soda lime glass substrates. We previously characterized the intermetallic phases in precursor films deposited by successive sputtering of elemental Cu, Ga, and In layers or using the $Cu_{0.8}Ga_{0.2}$ alloy sputter target [3]. The films were reacted with H_2Se at 450ºC for 15 or 30 minutes, followed by reaction in H_2S at 550 ºC for 15 or 30 minutes with , in all cases, an Ar/O_2 ambient.

All films formed by the 2-step reaction process were fully reacted, showing only XRD diffraction peaks from the chalcopyrite phase. AES composition depth profiles (measured by Craig Perkins at NREL) of these films are shown in Figure 7. They all show relatively uniform Cu profiles and steep S gradients near the film surface. The Ga and In profiles are dependent on selenization time. For 15-minute selenization, the films show nearly uniform Ga, while films selenized for 30 minutes show Ga accumulation at the back contact. In addition, the films

selenized for 15 minutes have 2 – 5 at% S throughout the bulk of the film while the films selenized for 20 minutes have < 1 at%. The effect of sulfization time is discernible but less dramatic. The films sulfized for 30 instead of 15 minutes show a 1.3 – 1.5x increase in surface S concentration. The high Cu concentration (>25%) measured by AES in all films was not corroborated by EDS, and is believed to be a systematic offset in the AES measurement, possibly resulting from preferential sputtering during the depth profiles.

The correlation between selenization time and Ga profile suggests that Ga distribution is fixed once it is incorporated in the chalcopyrite phase. With the longer selenization time, less of the Cu-Ga intermetallic is available for the sulfization reaction, and there is little Ga homogenization. If diffusion through the chalcopyrite is not the homogenization mechanism, then Ga mobility must occur externally to the chalcopyrite phase through secondary phases. Sulfur profiles near the surface of the four films are similar, though for a fixed selenization time, longer sulfization time yields higher surface sulfur concentration. Also, for the 15-minute selenized samples, the film sulfized for 30 minutes shows a higher bulk sulfur uptake than the film sulfized for 15 minutes. These observations are consistent with the low diffusivity of S into chalcopyrite $CuInSe_2$ unless secondary phases are present [4]. The only detectable bulk S incorporation occurs in the samples selenized for 15 minutes that have been reacted to a lesser degree than samples selenized for 30 minutes.

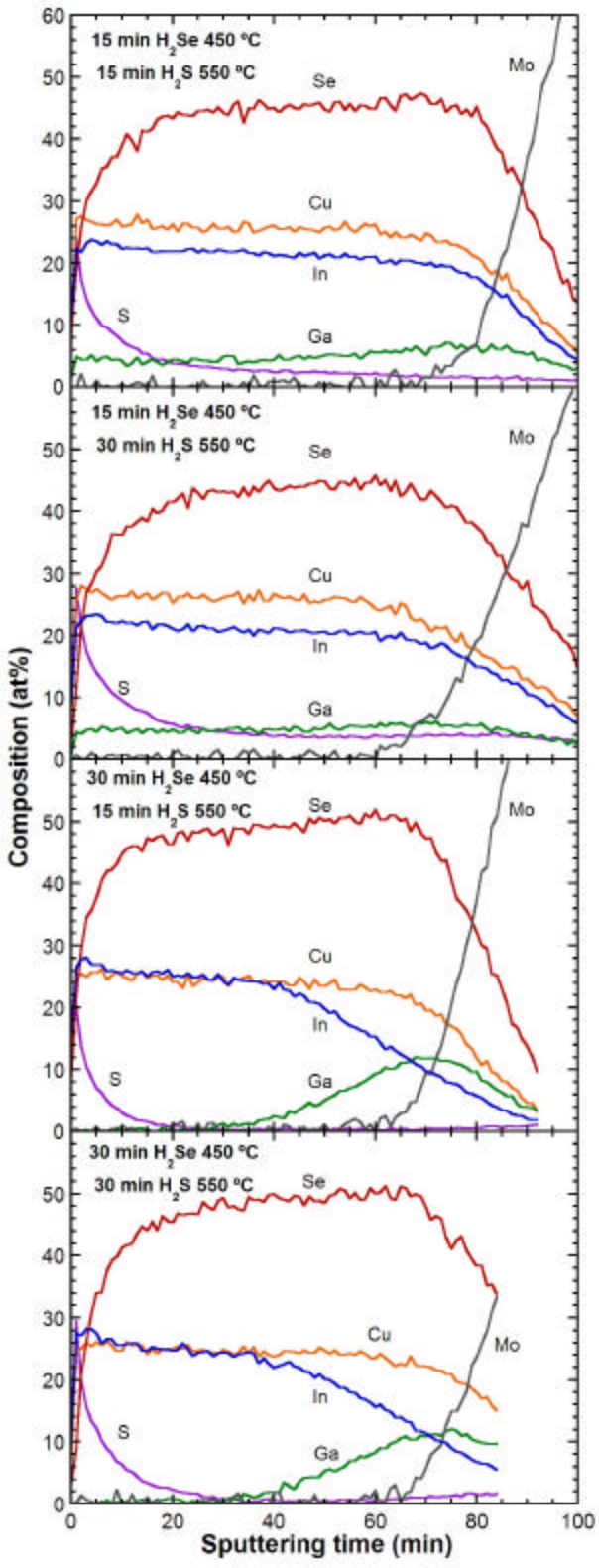

Figure 7. Comparison of AES depth profiles for films selenized for 15/30 minutes, then sulfized for 15/30 minutes.

Fundamental Materials and Interface Characterization

$Cu(InGa)Se_2$ Thickness

We previously reported characterization of the effect of absorber layer thickness (d) on device behavior using an aqueous Br-etch for different times to controllably reduce the thickness from 2.0 to 0.4 μm [3]. For comparison, a set of evaporation runs was done with different deposition times to change the thickness. The films were evaporated using a uniform process with no change in fluxes during the run. This process enables the thickness to be varied simply by changing the time, which the shutter between the sources and substrates is open. Optical reflection was measured and used to determine thickness as previously, and then devices were completed.

Figure 8 shows the device results comparing layers deposited for different times with the etched $Cu(InGa)Se_2$ layers. The thickness dependence of the cell parameters is mostly comparable to those obtained by Lundberg [5]. There is some scatter in V_{OC}, but no evidence for a decrease except for $d < 0.5$ μm. The decrease in J_{SC} for $d < 1$ μm is expected due to incomplete absorption, but is greater than predicted by device models [5,6]. The lack of any difference in J_{SC} between the etched and deposited thin layers suggests that the unaccounted loss in current is not due to light scattering effects which would be greater with the deposited layers. The etched absorber films gave FF ~ 75 % for all thicknesses down to 0.4 μm. This indicates that the loss in J_{SC} is not caused by poor collection, which would also reduce FF. Devices with the deposited thin layers had a decrease in FF for $d < 0.7$ μm, which may be related to surface roughness and thickness non-uniformity.

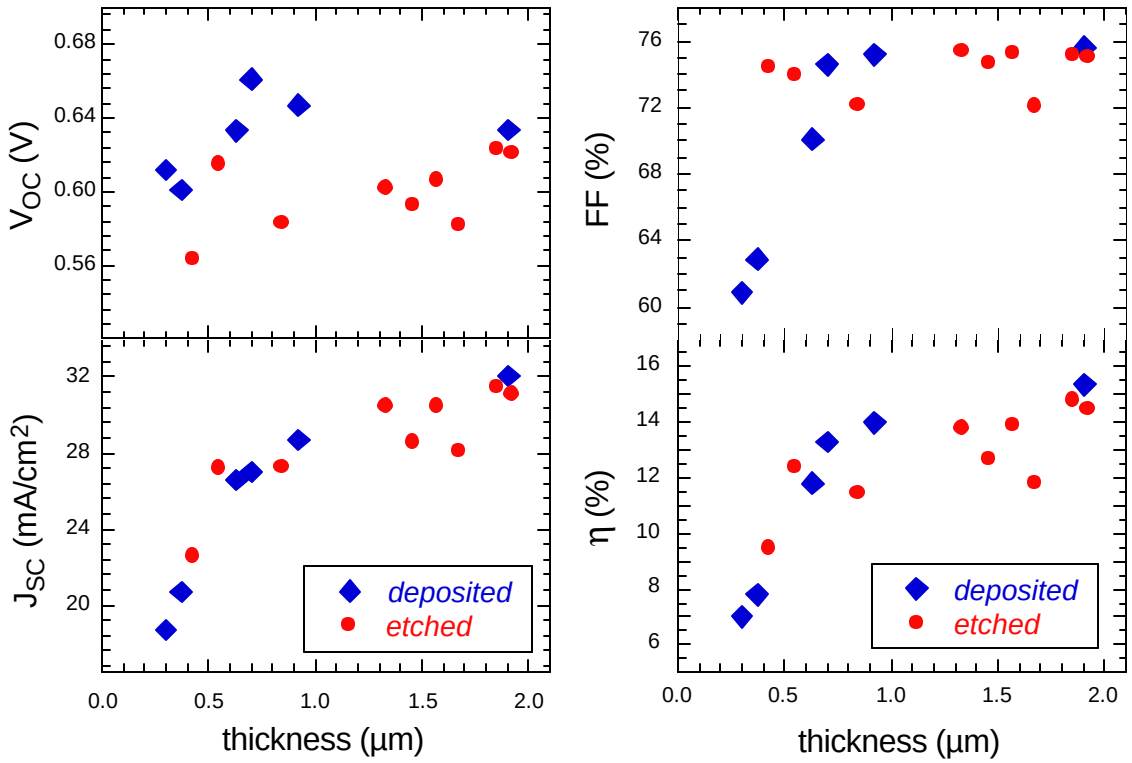

Figure 8. J-V parameters comparing devices with etched Cu(InGa)Se_2 and with as-deposited absorber layers grown for different times.

Cu(InGa)Se_2/Mo Back Contact

The formation of a $MoSe_2$ layer at the back contact between Mo and Cu(InGa)$(SeS)_2$ has been well documented [7] and can be a source of adhesion problems. Experiments have been done to characterize the reaction of Mo with H_2Se and H_2S to understand the back contact formation in the process of forming Cu(InGa)$(SeS)_2$ with reaction in the hydride gases. Sputtered Mo films on soda lime glass substrates were reacted for 1 hour in flowing H_2Se, H_2S, or an equal mixture of the two. In each case, the reaction was done at 550°C for 1 hour with a total hydride gas concentration of 0.35% in Ar.

Symmetric θ – 2θ XRD spectra, measured under Cu K_α radiation, of the three reacted films are shown in Figure 9. The film reacted in H_2Se has peaks corresponding to Mo and $MoSe_2$. The film reacted in H_2S only shows peaks from unreacted Mo. Finally, the film reacted in the mixed gas is similar to the film reacted in just H_2Se, though with lower intensity of the $MoSe_2$ peaks. The peak positions for the $MoSe_2$ phase show no shift which would indicate the formation of a $Mo(SeS)_2$ phase. While several peaks are indexed as $MoSe_2$, the strongest peak in the powder diffraction pattern, corresponding to the (103) reflection, was not observed. This would be expected at $2\theta = 37.9°$.

The films reacted in H_2S had a blue appearance, indicating that there was a surface layer so the films were examined more closely using glancing incident angle XRD as shown in Figure 10. In

this case, the films reacted in H_2Se and $H_2Se + H_2S$ show peaks from $MoSe_2$, including (103) reflection. The film reacted in H_2S shows MoS_2 (002) and (100) reflections that are shifted from the $MoSe_2$ (002) peak in the other 2 films. The measurements were done at incident angles of 0.7 and 1.0° corresponding to sampling depths of ~ 190 and 270 nm. Only the film reacted in H_2S shows Mo peaks, indicating that the MoS_2 is << 190 nm thick while the $MoSe_2$ layers are > 270 nm thick.

Finally, preliminary results have been obtained with Mo films deposited on Na-free borosilicate glass and reacted under the same conditions. The symmetric XRD results are similar to those on soda lime glass except changes in $MoSe_2$ orientation.

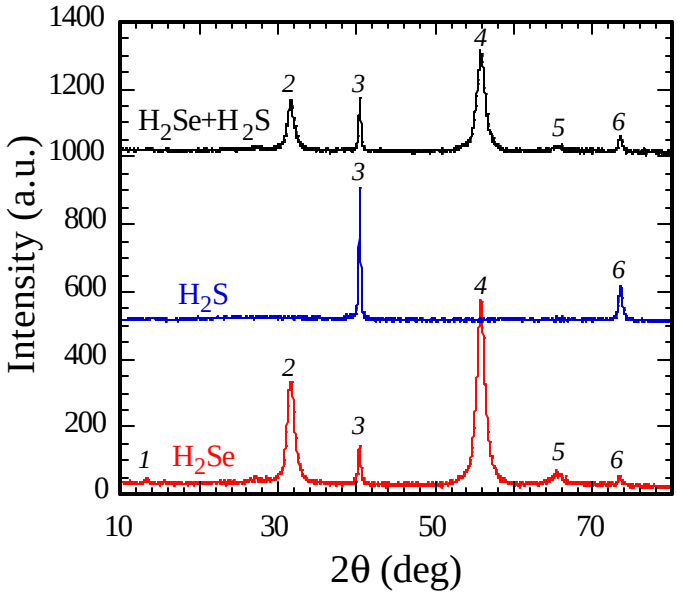

Figure 9. XRD spectra of Mo films reacted in H_2Se, H_2S, and a mixture of H_2Se and H_2S. Peaks are indexed as: *1* – $MoSe_2$ (002), *2* – $MoSe_2$ (100), *3* - Mo (110), *4* – $MoSe_2$ (110), *5* – $MoSe_2$ (200), *1* – Mo (211),

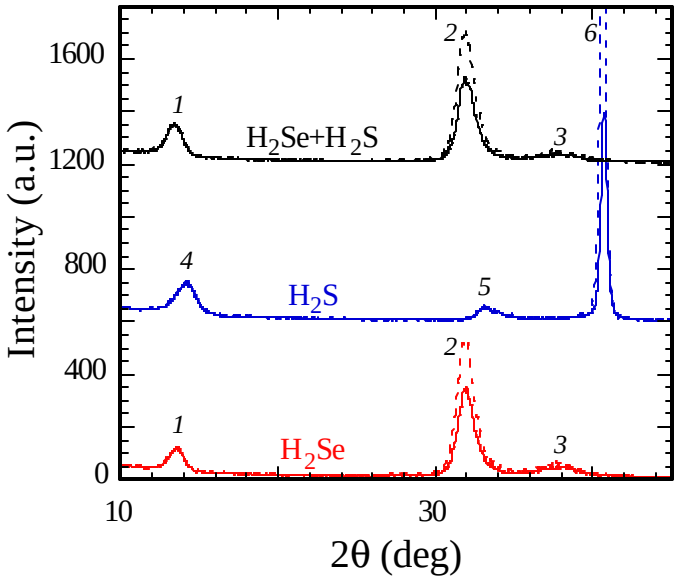

Figure 10. XRD spectra of Mo films reacted in H_2Se, H_2S, and a mixture of H_2Se and H_2S. Solid lines were measured at 0.7° incident angle and the dashed lines at 1.0°. Peaks are indexed as: *1* – $MoSe_2$ (002), *2* – $MoSe_2$ (100), *3* – $MoSe_2$ (103), 4 – MoS_2 (002), 5 – MoS_2 (100), *4* - Mo (110).

References

1. Y. Nagoya et al., *Solar Energy Mat. and Solar Cells* **67**, 247 (2001).
2 V. Alberts et al., *Thin Solid Films* **451-452**, 207 (2004).
3. Dec. 05 report – this contract
4. M. Engelmann, B. E. McCandless and R. W. Birkmire, *Thin Solid Films* **387**, 14 (2001).
5. O. Lundberg, M. Bodegard, J. Malmstrom L. Stolt, *Prog. Photovolt* **11**, 77 (2003).
6. M. Gloeckler, J. Sites, *J. Appl. Phys.* **98**, 103713 (2005).
7. S. Nishiwaki, N. Kohara, T.Negami, T. Wada, *Jpn. J. Appl. Phys.* **37**, L71 (1998).

Best regards,

Robert W. Birkmire
Director

cc: Susan Tompkins, UD Research Office
Carolyn Lopez, NREL